Molecular Therapy
Methods & Clinical Development
Original Article

In vivo genome editing at the albumin locus to treat methylmalonic acidemia

Jessica L. Schneller,[1] Ciaran M. Lee,[2] Leah E. Venturoni,[1] Randy J. Chandler,[1] Ang Li,[2] Sangho Myung,[1] Thomas J. Cradick,[3,5] Ayrea E. Hurley,[4] William R. Lagor,[4] Gang Bao,[2] and Charles P. Venditti[1]

[1]National Human Genome Research Institute, NIH, Bethesda, 20892 MD, USA; [2]Department of Bioengineering, Rice University, Houston, TX 77005, USA; [3]Georgia Institute of Technology, Atlanta, GA 30332, USA; [4]Department of Molecular Physiology and Biophysics, Baylor College of Medicine, Houston, TX 77030, USA

Methylmalonic acidemia (MMA) is a metabolic disorder most commonly caused by mutations in the methylmalonyl-CoA mutase (*MMUT*) gene. Although adeno-associated viral (AAV) gene therapy has been effective at correcting the disease phenotype in MMA mouse models, clinical translation may be impaired by loss of episomal transgene expression and magnified by the need to treat patients early in life. To achieve permanent correction, we developed a dual AAV strategy to express a codon-optimized *MMUT* transgene from *Alb* and tested various CRISPR-Cas9 genome-editing vectors in newly developed knockin mouse models of MMA. For one target site in intron 1 of *Alb*, we designed rescue cassettes expressing MMUT behind a 2A-peptide or an internal ribosomal entry site sequence. A second guide RNA targeted the initiator codon, and the donor cassette encompassed the proximal albumin promoter in the 5′ homology arm. Although all editing approaches were therapeutic, targeting the start codon of albumin allowed the use of a donor cassette that also functioned as an episome and after homologous recombination, even without the expression of Cas9, as an integrant. Targeting the albumin locus using these strategies would be effective for other metabolic disorders where early treatment and permanent long-term correction are needed.

INTRODUCTION

Methylmalonic acidemia (MMA) is a prototypical autosomal-recessive metabolic disease, most commonly caused by mutations in the gene coding for methylmalonyl-CoA mutase (*MMUT*), the terminal enzyme in the catabolic pathway of isoleucine, valine, odd-chained fatty acids, cholesterol, and propionate oxidation.[1] As with other severe metabolic disorders of infancy and childhood, treatment options remain limited, and long-term outcomes guarded.[2] The crux of disease management continues to be the dietary restriction of metabolic pathway precursors,[3] and aggressive management of intercurrent illnesses.[3,4] However, even with vigilant monitoring, MMA is associated with increased morbidity and mortality due to acute and chronic multi-systemic disease manifestations. The guarded prognosis of MMA has led to the use of elective liver transplantation increasingly at younger ages, to improve survival and delay long-term disease complications.[5–8] Successful liver transplant eliminates the propensity toward metabolic instability characteristic of MMA and related organic acidemias, but carries the need for lifelong immune suppression and the risk of developing transplant-related complications, including post-transplant lymphoproliferative disorder.[9] Thus, there is a great need for non-invasive therapies that could provide sufficient hepatic enzyme activity, that ideally would persist for the life of the affected individual.[10]

In an effort to establish new treatments for MMA, we previously developed a number of new genomic therapies, including recombinant adeno-associated viral (rAAV) gene therapy and systemic *MMUT* mRNA therapy.[11–14] Both approaches have intrinsic limitations related to the transient nature of expression, untoward immune reactions that might limit re-administration and, in the case of rAAV, the potential for genotoxicity caused by random integration of vectors containing strong promoter elements.[15] A distinct strategy to circumvent the limitations of transient and ectopic *MMUT* expression would be to use genome editing to target the insertion of a *MMUT* cDNA to a safe harbor locus, an area of the genome that can be manipulated without adverse effects, allowing for stable transgene expression in the liver. This strategy would provide the corrective benefit of conventional rAAV gene therapy, while enabling permanent correction after a single treatment.

To examine genome editing as a treatment for MMA in newly constructed knockin mouse models that recapitulate severe (mut^0) and partial (mut^-) deficiency forms of the disorder, we targeted the safe harbor locus *albumin* (*Alb*). AAV delivery of therapeutic *MMUT* donor cassettes, either into the first intron of *Alb*, or at the initiator codon in exon 1 of *Alb* with or without Cas9 endonuclease, provided pronounced clinical and biochemical effects. Targeting the 5′ end of *albumin* using the strategies described here can be readily applied to other metabolic disorders, and the nuclease-free insertion approach targeting at the *albumin* start codon may fully harness the potential for episomal expression of the donor cassette,

Received 29 September 2021; accepted 8 November 2021;
https://doi.org/10.1016/j.omtm.2021.11.004.

[5]Present address: Excision BioTherapeutics, 499 Jackson Street, San Francisco, CA 94111, USA

Correspondence: Charles P. Venditti MD, PhD, National Human Genome Research Institute, NIH, Bethesda, 20892 MD, USA.
E-mail: venditti@mail.nih.gov

circumvent genotoxic off-target activity,[15] and protect against untoward effects from pre-existing immunity to Cas9 orthologs.[16]

RESULTS

Murine models of MMA recapitulate patient phenotypes and respond to conventional AAV gene therapy

To model the diversity of pathogenic human mutations and phenotypes,[17] and their corresponding murine phenotypes, we used CRISPR-Cas9 genome editing to knock in characteristic *mut*^{o} (MMUT p.R108C) or *mut*$^{-}$ (MMUT p.G717V) missense mutations (Figure 1A) at the orthologous positions in the *Mmut* gene. We then characterized the clinical and biochemical phenotypes of mice with homozygous missense *Mmut* alleles, and established the response to conventional AAV gene addition therapy.

Mmut$^{p.R106C/p.R106C}$ and *Mmut*$^{p.G715V/p.G715V}$ mice were observed from birth and their survival compared with unaffected *Mmut*$^{+/p.R106C}$ and *Mmut*$^{+/p.G715V}$ littermates (Figures 1B and 1E). Less than 10% of *Mmut*$^{p.R106C/p.R106C}$ (n = 37) survived to day of life 57 (DOL57), with the greatest mortality observed during the first 2 weeks of life: more than half of the homozygous mutant mice perished (Figure 1E). After treatment at birth with an AAV serotype 9 vector expressing a human codon-optimized human MMUT from a ubiquitous promoter, the majority of the treated mutant *Mmut*$^{p.R106C/p.R106C}$ survived normally compared with carrier controls (Figure 1E). We similarly followed the survival of *Mmut*$^{p.G715V/p.G715V}$ and compared it with wild-type *Mmut*$^{+/p.G715V}$ littermates (Figure 1B). At 111 days, no significant difference in the mean survival was observed between healthy *Mmut*$^{+/p.G715V}$ and affected *Mmut*$^{p.G715V/p.G715V}$ mice, indicating that this MMA model does not exhibit disease-related mortality, similar to what we observed in a transgenic overexpression mouse model of this mutation.[18]

Because *Mmut*$^{p.R106C/p.R106C}$ mice manifested a more severe phenotype, with disease-associated lethality occurring predominantly in the first week of life, we euthanized a litter of *Mmut*$^{p.R106C/p.R106C}$ on DOL1 to measure methylmalonic acid concentrations. Indeed, we observed that plasma methylmalonic acid concentrations were massively elevated, with values of 2,931 ± 820.5 μM (Figure 1F), close to the values seen in *Mmut* exon 3 knockout mice sampled at a similar age.[19] After neonatal treatment with a dose of 1e11 GC/pup AAV9.EF1a.PI.MMUT.RBG, metabolite concentrations in *Mmut*$^{p.R106C/p.R106C}$ were significantly reduced, comparable with concentrations observed at age 1 year in *Mmut* exon 3 knockout mice treated at birth with a dose of either 1e11 GC/pup or 2e11 GC/pup of an AAV8 vector expressing murine Mmut from a chicken beta-actin promoter[20] (Figure 1F). In comparison, methylmalonic acid levels in the blood of *Mmut*$^{p.G715V/p.G715V}$ were significantly elevated compared with age-matched *Mmut*$^{+/p.G715V}$ controls, but much lower than the levels measured in younger *Mmut*$^{p.R106C/p.R106C}$ mice, with concentrations of 802.5 ± 218.7 μM at 16 weeks (Figure 1C).

Growth, as assessed by weight in *Mmut*$^{p.R106C/p.R106C}$ mice from age 1 month and in *Mmut*$^{p.G715V/p.G715V}$ from weaning, was measured to determine whether the clinical phenotype aligned with observations made from MMA patients, many of whom exhibit growth retardation. As expected, based on the mortality and biochemical parameters, *Mmut*$^{p.R106C/p.R106C}$ that survive beyond weaning were severely growth impaired, with weights that were 50% less than age-matched controls (Figure 1G).

During the first 4 months of life, *Mmut*$^{p.G715V/p.G715V}$ display retarded growth compared with wild-type *Mmut*$^{+/p.G715V}$ controls when fed a regular chow diet (Figure 1D). To assay the effects of traditional AAV gene therapy, a small cohort of *Mmut*$^{p.G715V/p.G715V}$ (n = 3) was treated with 5×10^{12} GC/kg of AAV8.EF1a.PI.MMUT.RBG gene, delivered via the retro-orbital plexus, at age 1 month. AAV8-treated *Mmut*$^{p.G715V/p.G715V}$ mice increased their body weight by an average of 45% within a week of treatment, and grew to be not significantly different in size from *Mmut*$^{+/p.G715V}$ littermates (Figure 1D). A brisk metabolic response also was noted, with plasma methylmalonic acid concentrations dropped by over 75% to less than 100 μM in *Mmut* $^{p.G715V/p.G715V}$ 3 weeks after treatment with AAV8.EF1a.PI.MMUT.RBG (Figure 1C).

Due to the high rate of mortality, only two *Mmut*$^{p.R106C/p.R106C}$ male mice were treated with systemic AAV8.EF1a.PI.MMUT.RBG gene therapy after weaning. By 15 days post-treatment, both MMA mice had doubled in weight to sizes not significantly different from unaffected littermates (Figure 1G). Because *Mmut*$^{p.R106C/p.R106C}$ further displayed pronounced lethality before weaning, we additionally performed a neonatal gene therapy study using an identical vector pseudotyped with an AAV9 capsid (Figure 1E). Rescue to weaning and growth correction beyond was observed, with mitigation of biochemical perturbations and a sparse pattern of MMUT mRNA expression in hepatocytes of treated *Mmut*$^{p.R106C/p.R106C}$ mice compared with mutant mice receiving genome-editing components (Figures 4E, 5E, and S4). In summary, these new MMA mouse models recapitulate the spectrum of severity of clinical and biochemical phenotypes seen in patients with the corresponding mutations, and respond to conventional AAV gene therapy, as neonates, juveniles, or adults, as has been noted in other mouse models of MMA.[11,13,20,21]

Therapeutic editing into the albumin locus

We identified target sites for the *Staphylococcus aureus* Cas9 guide RNAs in the 5′ end of the *albumin* locus (Figure S1A),[22] tested *in vitro* (Figures S1D and S1E), and then *in vivo* as described previously.[23] Next-generation sequencing across the native target demonstrated on-target indel formation at the Sa37 and Sa08 targets of ∼30% and ∼20%, respectively (Figure S1B), as well as rare evidence of integration of the AAV vector at the Sa37 site (Figure S1C). Next, we delivered dual vectors, including the SaCas9/gRNA at a dose of 5e10 GC per pup, and rescue cassettes containing a codon-optimized *MMUT* transgene at a dose of 2e11 GC per pup, to *Mmut*$^{p.R106C/p.R106C}$ and *Mmut*$^{p.G715V/p.G715V}$ mice and littermate controls treated as neonates. Treated MMA mice and wild-type heterozygote controls were aged to 9 months prior to sacrifice, and the clinical (weight and survival) and biochemical (plasma

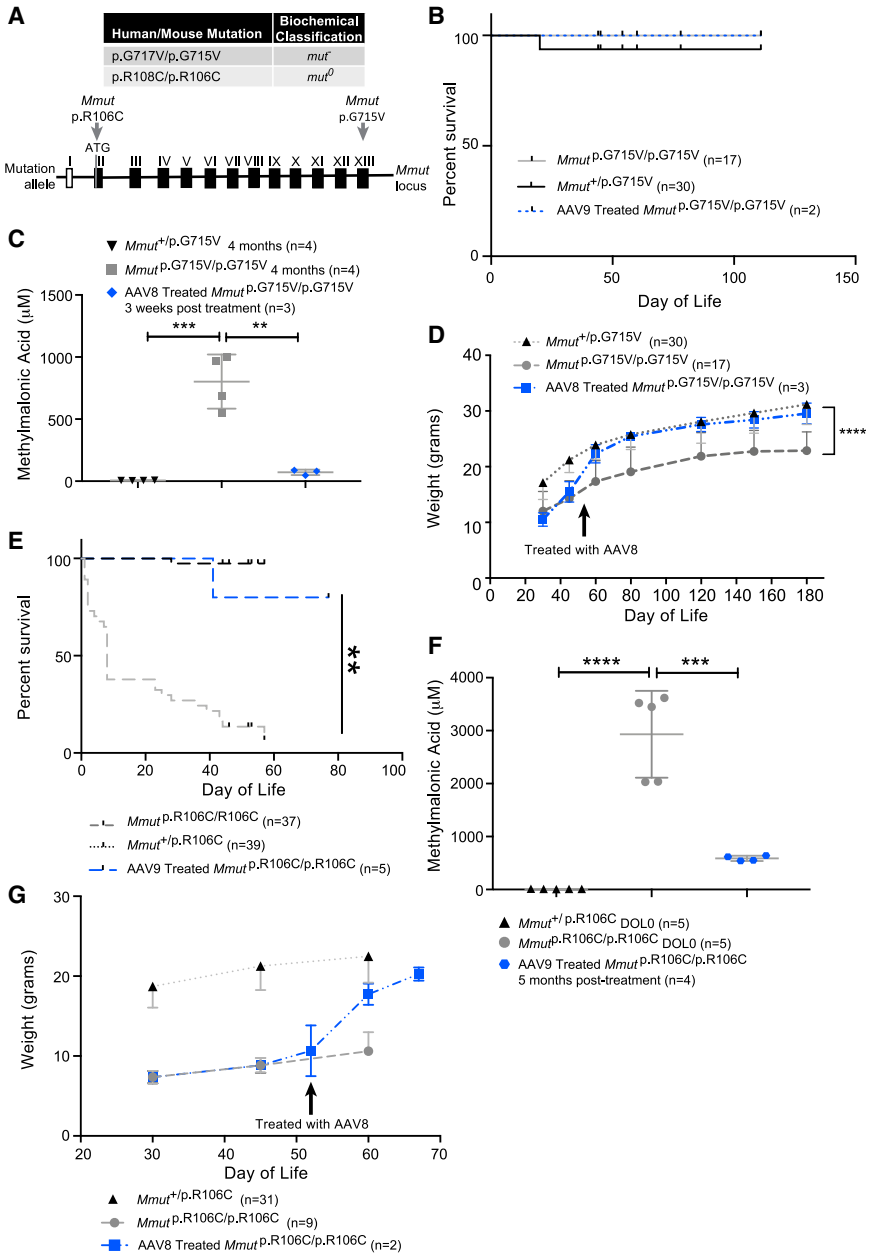

Figure 1. Phenotypic and biochemical characterization of MMA mouse models recapitulating patient missense mutations before and after treatment with therapeutic AAV8 or AAV9 vectors

(A) Murine *Mmut* alleles generated using CRISPR-Cas9 genome editing. MMUTp.R108C (murine Mmutp.R106C), located in the region coding for the substrate binding domain, is classified as mut^0: there is no detectable MMUT activity, resulting in the more common, and severe, form of the disorder. MMUTp.G717V (murine Mmutp.G715V) is located in the putative cofactor binding pocket and is classified as mut^-, exhibiting partial activity *in vitro*. (B) Survival of $Mmut^{p.G715V/p.G715V}$ mice. There was no significant difference in the mean survival between healthy $Mmut^{+/p.G715V}$ and diseased $Mmut^{p.G715V/p.G715V}$ mice. (C) Plasma methylmalonic acid concentrations in $Mmut^{p.G715V/p.G715V}$ mice. Plasma methylmalonic acid was significantly elevated in $Mmut^{p.G715V/p.G715V}$ compared with age-matched $Mmut^{+/p.G715V}$ controls at 16 weeks. Methylmalonic acid concentrations in $Mmut^{p.G715V/p.G715V}$ at 16 weeks treated with 5×10^{12} GC/kg AAV8.EF1a.PI.MMUT.RBG dropped significantly, by over 75%, 3 weeks post-treatment. (D) Growth trends in $Mmut^{p.G715V/p.G715V}$. Throughout the first 6 months of life, untreated $Mmut^{p.G715V/p.G715V}$ only reach ~70% of the weight of their $Mmut^{+/p.G715V}$ littermates. Treatment on DOL41 with 5×10^{12} GC/kg AAV8.EF1a.PI.MMUT.RBG led to increased body weight and growth comparable with $Mmut^{+/p.G715V}$ controls by DOL60. (E) Survival of $Mmut^{p.R106C/p.R106C}$ mice. Only 6% of $Mmut^{p.R106C/p.R106C}$ survived to DOL57; however, treatment of $Mmut^{p.R106C/p.R106C}$ mice at birth via retro-orbital injection with 1e11 GC/pup AAV9.EF1a.PI.MMUT.RBG rescued mutant mice from neonatal lethality. (F) Plasma methylmalonic acid concentrations in $Mmut^{p.R106C/p.R106C}$ mice on DOL0 are massively elevated compared with $Mmut^{+/p.R106C}$ littermates. After treatment at birth with 1e11 GC/pup AAV9.EF1a.PI.MMUT.RBG, methylmalonic acid concentrations in $Mmut^{p.R106C/p.R106C}$ were significantly reduced at age 5 months. (G) Growth trends in $Mmut^{p.R106C/p.R106C}$ mice for which untreated controls do not survive past 60 days. Untreated $Mmut^{p.R106C/p.R106C}$ mice that survived past weaning were severely growth impaired compared with $Mmut^{+/p.R106C}$ littermates at age 1 month, but treatment with 5×10^{12} GC/kg AAV8.EF1a.PI.MMUT.RBG on DOL52 improved growth to levels not significantly different from healthy $Mmut^{+/p.R106C}$ controls by DOL60. In (B) and (E), data were analyzed by log rank Mantel-Cox and Gehan-Breslow-Wilcoxon test. $^{**}p < 0.01$, versus the untreated $Mmut^{p.R106C/p.R106C}$ group. In (C) and (F), values are expressed as mean ± SD and analyzed by unpaired Student's t test. In (C), methylmalonic acid concentrations for untreated $Mmut^{p.G715V/p.G715V}$ (802.5 ± 218.7 µM), age-matched $Mmut^{+/p.G715V}$ (5.66 ± 1.60 µM, n = 4), and $Mmut^{p.G715V/p.G715V}$ treated with AAV8.EF1a.PI.MMUT.RBG (71.57 ± 22.09 µM, n = 3). In (F), methylmalonic acid concentrations in untreated $Mmut^{p.R106C/p.R106C}$ at birth (2,931 ± 820.5 µM, n = 5) compared with $Mmut^{+/p.R106C}$ littermates (11.07 ± 1.63 µM, n = 5), and 5 months post-treatment with AAV9.EF1a.PI.MMUT.RBG (588 ± 49.0 µM, n = 4). $^{***}p < 0.001$. In (D) and (G), weight values are expressed as mean ± SD and analyzed by unpaired Student's t test. At age 1 month, untreated $Mmut^{p.R106C/p.R106C}$ (7.35 ± 0.79 g) versus healthy $Mmut^{+/p.R106C}$ controls (18.72 ± 2.66 g, $^{****}p < 0.0001$). Adult $Mmut^{p.R106C/p.R106C}$ mice treated with 5×10^{12} GC/kg AAV8.EF1a.PI.MMUT.RBG on DOL52 improved growth to levels not significantly different from $Mmut^{+/p.R106C}$ littermates by DOL60 (17.7 ± 1.32 g for treated $Mmut^{p.R106C/p.R106C}$ versus 22.5 ± 3.30 g for $Mmut^{+/p.R106C}$).

methylmalonic acid concentration) phenotypes were assessed. Cohorts of treated mutant mice were also allowed to age beyond the 9-month time point to examine the long-term safety profile after genome editing.

Correction with donor constructs targeting albumin intron 1 (Sa37)

Donor cassettes were designed using a human codon-optimized human MMUT cDNA in *cis* with either a 2A peptide or internal

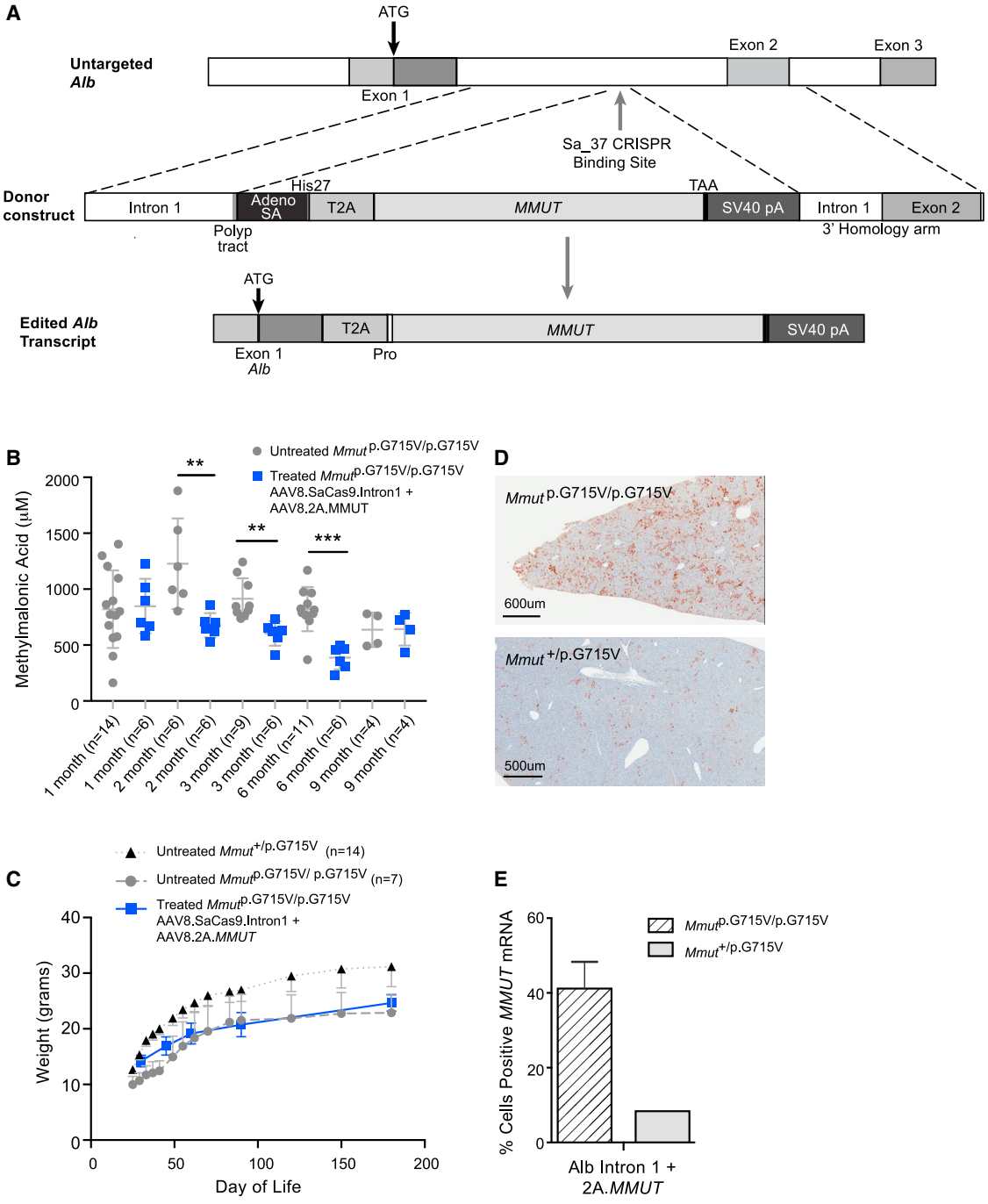

Figure 2. AAV8.2A.MMUT.SV40 targeted to *Alb* intron 1 leads to *MMUT* mRNA expression and reduced methylmalonic acid concentrations in *Mmut*$^{p.G715V/p.G715V}$

(A) Schematic of the donor construct corresponding to the Sa37 gRNA, targeting intron 1 of *Alb*. 2A-peptide precedes a full-length, human codon-optimized methylmalonyl-CoA mutase cDNA. (B) Plasma methylmalonic acid concentrations for *Mmut*$^{p.G715V/p.G715V}$ treated with 5e10 GC/pup AAV8.HLP.SaCas9.Sa37 + 2 × 10^{11} GC/pup AAV8.2A.MMUT.SV40 at birth, compared with untreated *Mmut*$^{p.G715V/p.G715V}$ at age 1, 2, 3, 6, and 9 months (terminal). At 1 month, no reduction in plasma methylmalonic acid was observed in the treated mice. At 2 months, a significant difference was observed in methylmalonic acid in untreated versus treated mice, which persisted until sacrifice at 9 months. (C) Weights of *Mmut*$^{p.G715V/p.G715V}$ treated with AAV8.HLP.SaCas9.Sa37 + AAV8.2A.MMUT.SV40 compared with untreated *Mmut*$^{p.G715V/p.G715V}$ and untreated *Mmut*$^{+/p.G715V}$ mice at 1 month and 45 days, and 2, 3, and 6 months. At 1 month, weights of treated *Mmut*$^{p.G715V/p.G715V}$ were significantly larger than untreated *Mmut*$^{p.G715V/p.G715V}$, but by age 2 months were not significantly different than untreated *Mmut*$^{p.G715V/p.G715V}$ mice, and were significantly smaller in size than heterozygous *Mmut*$^{+/p.G715V}$ controls at all subsequent time points. The growth data shown from these experiments include time points for which we had relevant untreated

(legend continued on next page)

ribosomal entry site (IRES) sequence (Figures 2A and 3A), with *Alb* homology arms of ~400 bp on either side of the insert.

Plasma methylmalonic acid concentrations and growth in treated *Mmut*$^{p.G715V/p.G715V}$ remained elevated at age 1 month, but became significantly reduced beginning at the 2-month time point, and continued to decrease during subsequent time points (Figure 2B). Some of the treated mutant mice exhibited elevated levels of plasma metabolites during the terminal bleed at 9 months due to the stress of euthanasia, an effect observed for all genome-editing strategies (Figures 2B, 3B, and 4C). One month after editing, treated *Mmut*$^{p.G715V/p.G715V}$ mice were significantly larger in size than untreated *Mmut*$^{p.G715V/p.G715V}$ controls, and similar in size to heterozygous littermates (Figure 2C). However, as the mice aged, they did not achieve the weight of the heterozygous-treated control littermates.

To validate on-target integration of the AAV8.2A.MMUT.SV40 donor, we developed a PCR assay of the 5′ integration junction from liver genomic DNA of treated *Mmut*$^{p.G715V/p.G715V}$ mice and untreated controls. Successful amplification indicated that integration had occurred in the treated, but not the untreated mice (Figure S2D). RNA *in situ* hybridization assay using a specific probe to detect the human codon-optimized *MMUT* mRNA showed significantly less staining in treated *Mmut*$^{+/p.G715V}$ livers compared with treated *Mmut*$^{p.G715V/p.G715V}$ mice (Figures 2D and 2E), consistent with previous observations suggesting that corrected hepatocytes display a growth advantage in the environment of an MMA liver.[24] Similar studies with an AAV8.IRES.MMUT.SV40 donor construct were performed, and likewise documented a biochemical and growth response seen only in the treated *Mmut*$^{p.G715V/p.G715V}$ mice (Figures 3 and S2E). In summary, Cas9-mediated insertion of either an AAV8.2A.MMUT.SV40 or an AAV8.IRES.MMUT.SV40 donor in the first intron of *albumin* resulted in targeted integration of the rescue cassette, leading to a sustained reduction in methylmalonic acid concentrations, and an improvement in growth in treated *Mmut*$^{p.G715V/p.G715V}$, with a concomitant expansion of the edited hepatocytes.

MMUT expression after editing at the start codon of albumin

We next assessed an alternate strategy targeting integration of a *MMUT* cDNA to the *albumin* start codon (gRNA designated Sa08) in the more severe MMA mouse model, *Mmut*$^{p.R106C/p.R106C}$ (Figure 4A and S2F). Because the 5′ homology arm of the donor contains part of the *albumin* promoter, immediate and substantial levels of expression from episomes of the AAV donor cassette were expected prior to *MMUT* integration. We were therefore able to assess the potential for this genome-editing strategy to rescue mice with more severe MMA phenotypes requiring immediate *MMUT* expression.

Because *Mmut*$^{p.R106C/p.R106C}$ exhibit disease-associated mortality early in life, we first assessed efficacy of editing at the start codon by looking for improvement in survival (Figure 4B). Strikingly, 75% of mutant *Mmut*$^{p.R106C/p.R106C}$ treated at birth survived to the experimental endpoint of 9 months. Plasma metabolites were significantly reduced in treated *Mmut*$^{p.R106C/p.R106C}$ compared with control values (Figure 4C), and treated *Mmut*$^{p.R106C/p.R106C}$ were significantly larger than untreated *Mmut*$^{p.R106C/p.R106C}$ controls at age 1 month (Figure 4D), reaching the size of untreated *Mmut*$^{+/p.R106C}$ littermates, an effect that was sustained for the duration of the study.

Untreated *Mmut*$^{p.R106C/p.R106C}$ and *Mmut*$^{p.G715V/p.G715V}$ mice produce immunoreactive Mmut protein in their livers (Figures S3A and S3B), yet treated *Mmut*$^{p.R106C/p.R106C}$ exhibited a relative increase in protein expression for 9 months after treatment (Figure S3C). RNA *in situ* hybridization results indicated that ~50% of hepatocytes were expressing *MMUT* mRNA in treated *Mmut*$^{p.R106C/p.R106C}$ at 9 months post-treatment, greatly increased compared with the treated *Mmut*$^{+/p.R106C}$ littermate (Figures 4E and 4F), and even ~10% higher than the corresponding values seen in *Mmut*$^{p.G715V/p.G715V}$ mice treated with the AAV8.SaCas9.Sa37 and either the AAV8.2A.MMUT.SV40 or AAV8.IRES.MMUT.SV40 constructs. On-target integration of the *MMUT* donor was supported by integration junction amplification noted only in the Sa08-treated mice (Figure S2F), with *MMUT* genome copy numbers higher in treated *Mmut*$^{p.R106C/p.R106C}$ compared with mice treated with AAV8.SaCas9.Sa37 and either the AAV8.2A.MMUT.SV40 or AAV8.IRES.MMUT.SV40 constructs at 9 months post-treatment (Figures S2A–S2C).

Nuclease-free genome editing at the albumin start codon in *Mmut*$^{p.R106C/P.R106C}$

To examine whether the significant therapeutic effects of genome editing at the *albumin* ATG were due to episomal donor vector expression, we treated a cohort of *Mmut*$^{p.R106C/p.R106C}$ mice at birth with the AAV8.MMUT.SV40 donor-only, at the dose used in dual-vector studies (2e11 GC/pup), but without the Cas9 vector (Figure 5A). We observed significant rescue from disease-related neonatal mortality in *Mmut*$^{p.R106C/p.R106C}$ treated with AAV8.MMUT.SV40 donor-only

Mmut$^{p.G715V/p.G715V}$ and *Mmut*$^{+/p.G715V}$ control data. (D) Liver sections from treated *Mmut*$^{p.G715V/p.G715V}$ mice and one treated *Mmut*$^{+/p.G715V}$ control were stained for *MMUT* mRNA using a probe specific to the transgene. (E) Expression of *MMUT* mRNA at 9 months was in the liver of edited *Mmut*$^{p.G715V/p.G715V}$ mice. Positively stained cells were evenly distributed throughout the liver. A *Mmut*$^{+/p.G715V}$ littermate control treated with AAV8.HLP.SauCas9.Sa37 + AAV8.2A.MMUT.SV40 exhibited only a small number of cells with positive mRNA staining at 9 months. In (B), plasma methylmalonic acid concentrations were analyzed by unpaired Student's t test as mean ± SD. Methylmalonic acid values at 1 month in treated *Mmut*$^{p.G715V/p.G715V}$ mice (848.3 ± 99.38 μM) were comparable with untreated *Mmut*$^{p.G715V/p.G715V}$ (820.3 ± 92.6 μM), but were significantly reduced in treated mice for later time points. **$p < 0.01$, ***$p < 0.001$, versus the untreated *Mmut*$^{p.G715V/p.G715V}$ group. In (C), weight values are expressed as mean ± SD and analyzed by unpaired Student's t test. At 1 month, treated *Mmut*$^{p.G715V/p.G715V}$ were significantly larger than untreated *Mmut*$^{p.G715V/p.G715V}$ ($p = 0.0001$). In (E), *MMUT* mRNA expression was quantified as percentage of hepatocytes stained positive and expressed as mean ± SEM. At 9 months edited *Mmut*$^{p.G715V/p.G715V}$ mice exhibited 41.19% ± 3.56% *MMUT*-positive cells in the liver. The treated *Mmut*$^{+/p.G715V}$ control exhibited 8.40% of hepatocytes with positive mRNA staining at this time point.

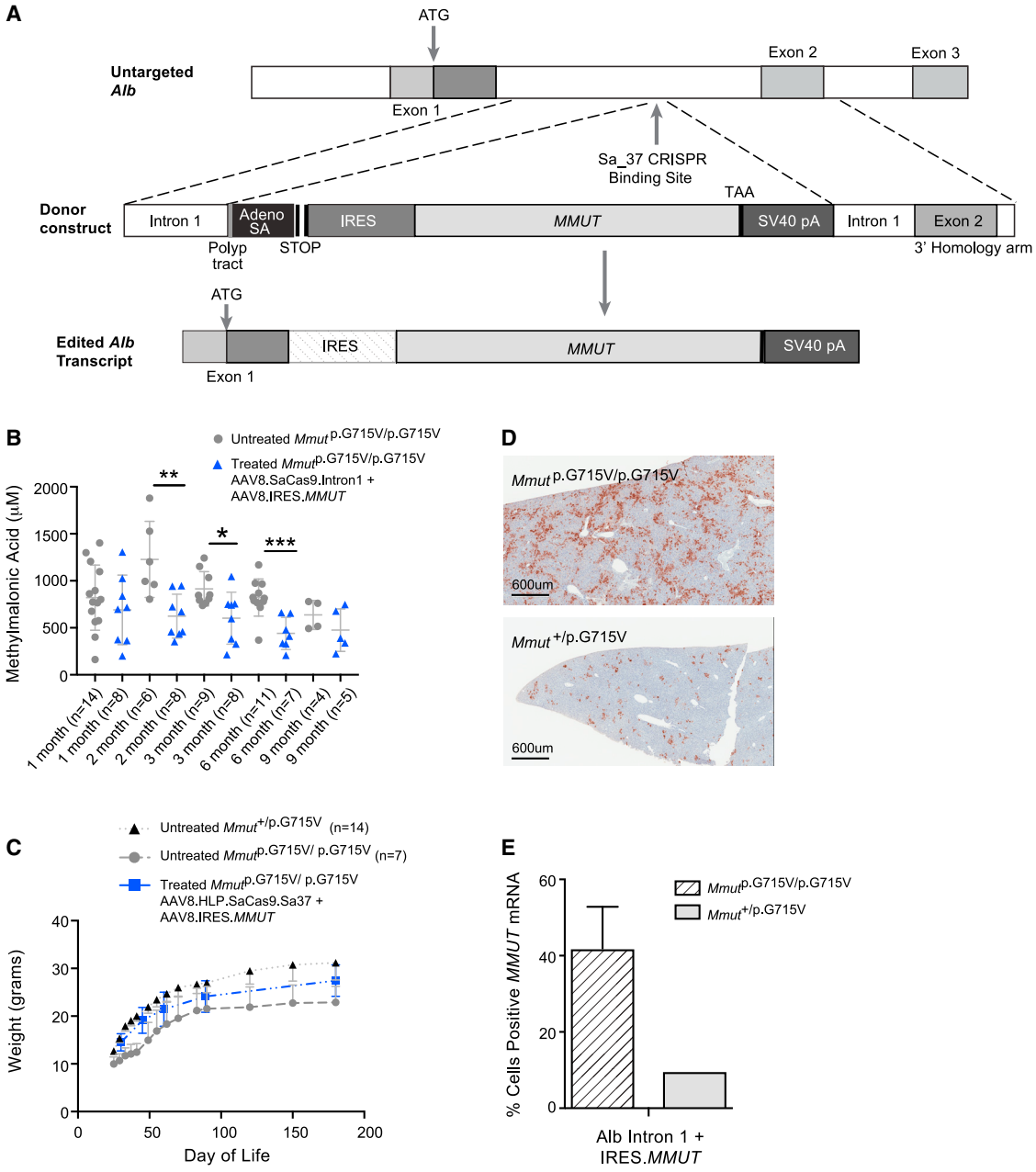

Figure 3. Targeting an AAV8.IRES.MMUT cassette into *Alb* intron 1 results in *MMUT* mRNA expression and improves clinical outcomes in *Mmut*$^{p.G715V/p.G715V}$

(A) Schematic of the donor construct corresponding to the Sa37 gRNA targeting intron 1 of *Alb*. (B) Plasma methylmalonic acid concentrations for *Mmut*$^{p.G715V/p.G715V}$ administered AAV8.HLP.SaCas9.Sa37 + AAV8.IRES.MMUT.SV40 at birth, compared with untreated *Mmut*$^{p.G715V/p.G715V}$ controls at 1, 2, 3, 6, and 9 months (terminal). At 1 month, no reduction in plasma methylmalonic acid was observed in treated versus untreated mice. At 2 months, a significant difference was observed in methylmalonic acid in untreated versus treated mice which persisted. (C) Weights for *Mmut*$^{p.G715V/p.G715V}$ treated with 5e10 GC/pup AAV8.HLP.SauCas9.Sa37 + 2 × 10^{11} GC/pup AAV8.IRES.MMUT.SV40 compared with untreated *Mmut*$^{p.G715V/p.G715V}$ and untreated *Mmut*$^{+/p.G715V}$ mice at 1 month and 45 days, and 2, 3, and 6 months. Treated *Mmut*$^{p.G715V/p.G715V}$ were comparable in size with heterozygous *Mmut*$^{+/p.G715V}$ controls for all time points. The growth data shown from these experiments include time points for which we had relevant untreated *Mmut*$^{p.G715V/p.G715V}$ and *Mmut*$^{+/p.G715V}$ control data. (D) Liver sections from treated *Mmut*$^{p.G715V/p.G715V}$ were stained for *MMUT* mRNA using a transgene-specific probe. (E) Expression of *MMUT* mRNA in treated *Mmut*$^{p.G715V/p.G715V}$ at 9 months. Treated *Mmut*$^{p.G715V/p.G715V}$ exhibited an even distribution of positively stained cells throughout the liver. One *Mmut*$^{+/p.G715V}$ littermate control treated with 5e10 GC/pup AAV8.HLP.SauCas9.Sa37 + 2 × 10^{11} GC/pup AAV8.IRES.MMUT.SV40 exhibited significantly fewer positively stained hepatocytes at 9 months. In (B), plasma methylmalonic acid concentrations were analyzed by

(legend continued on next page)

compared with untreated *Mmut*$^{p.R106C/p.R106C}$ controls, with 85% of treated mice surviving normally compared with *Mmut*$^{+/p.R106C}$ controls ($p < 0.001$ compared with untreated *Mmut*$^{p.R106C/p.R106C}$ controls, log rank Mantel-Cox test) (Figure 5B). RNA *in situ* hybridization results indicated that ~24% of hepatocytes were expressing the *MMUT* mRNA in treated *Mmut*$^{p.R106C/p.R106C}$ at 5 months post-treatment, compared with <1% in a treated *Mmut*$^{+/p.R106C}$ at 5 months (Figures 5E and 5F). Corresponding with the improvement in survival, plasma methylmalonic acid concentrations were significantly reduced at age 2 months in the donor-only-treated *Mmut*$^{p.R106C/p.R106C}$ and were not significantly different than values from *Mmut*$^{p.R106C/p.R106C}$ treated with the dual Cas9 and donor vectors, at the same time point (Figure 5C). Donor-only-treated *Mmut*$^{p.R106C/p.R106C}$ were significantly larger in size than untreated *Mmut*$^{p.R106C/p.R106C}$ controls at 2 months, but were smaller in size than *Mmut*$^{p.R106C/p.R106C}$ treated with the dual-vector strategy (Figure 5D).

DISCUSSION

To expand upon existing mouse models of MMA, we used CRISPR-Cas9 genome editing to knock in missense mutations observed in *mut*^{0} and *mut*$^-$ MMA patients. These new models recapitulate key disease parameters identified in existing knockout and transgenic MMA mouse models, such as growth impairment, massively elevated levels of disease metabolites, and substantial lethality in the *mut*^{0} missense model.[14,19,21,25–30] While most previous mouse models harbor selection cassettes or synthetic elements, the new alleles presented here are transgene and deletion free. In addition to recapitulating features of the patients with corresponding mutations, these mice respond to gene therapy using conventional AAV vectors, showing improvements in survival and growth, and reduction of metabolites, similar to what we have observed from studies performed in knockout and transgenic MMA mouse models.[11,13,20,21]

Due to the transient therapeutic effects associated with episomal transgene expression when AAV is delivered in the neonatal period, and the potential for genotoxicity when AAV vector integration occurs randomly,[15] we relied upon editing into *albumin*, which has been employed for several metabolic disorders with variable success.[10] Targeting the 5′ end of *albumin* using zinc finger nucleases (ZFNs)[31] has entered human trials for Hunter syndrome, and efficiency of the ZFN strategy has been enhanced using CRISPR-Cas9 in treatment of mucopolysaccharidosis type I.[32] Editing the 3′ end of *albumin* preserves *albumin* expression, but current applications rely upon the fusion of *albumin* to the inserted transgene via a 2A peptide, which adds foreign 2A amino acids to the C terminus of *albumin*, and a proline to the gene of interest.[24,33] Some proteins will tolerate such alteration, but whether the resultant Alb-2A produced by editing at the 3′ end of *albumin* might engender an antibody formation or elicit a T cell response remains unknown, and potentially, a limiting toxicology consideration. Furthermore, the low efficiency of homologous recombination with nuclease-free approaches, and very high AAV doses required for efficacy, may further present a hurdle as has been demonstrated by the need for Cas9 to improve the efficacy of 3′ transgene insertion into the *albumin* locus in treatment of Crigler-Najjar syndrome mouse models.[34,35] For these reasons, we selected the CRISPR-Cas9 genome-editing system to enable efficient transgene integration near the site previously targeted by ZFN editing, and then further focused our efforts at the *albumin* start codon. The programmability of the CRISPR-Cas9 system allowed the design and testing of several guides, with two then selected for further *in vivo* application.

After *in vitro* and *in vivo* characterization of the lead guides, we designed several DNA donor cassettes to edit the *albumin* locus that utilized either a 2A peptide or an IRES sequence preceding the *MMUT* coding sequence in the donor construct, inserted into intron 1 of *albumin*. While the correction with both cassettes was substantial, and durable, the biochemical parameters in the treated MMA mice showed less correction than seen with conventional AAVs (Figure 1), suggesting that the editing approach might be further improved. We then targeted a *MMUT* cDNA to the start codon of *albumin*, encouraged by the lack of off-target effects seen with the Sa08 guide (Figure S1F) and the potential for immediate transgene expression before integration due to the presence of the *albumin* promoter in the 5′ homology arm of the donor, and used a more severely affected mouse model to assess therapeutic benefit. Indeed, the rescue from lethality and reduction of metabolites was comparable between nuclease plus donor- and donor-only-treated *Mmut*$^{p.R106C/p.R106C}$ mice. Furthermore, the morphologic pattern of *MMUT* mRNA expression in livers harvested from donor-only-treated mice revealed clusters of cells that further yielded a PCR product that could only be generated after successful homologous recombination, is consistent with the clonal expansion after homologous recombination, and similar to what has been seen in other studies,[24,33,35–38] suggesting that AAV-mediated, nuclease-free homologous recombination was responsible for the long-term therapeutic effects. While we were unable to measure homology-directed repair (HDR) versus non-homologous end joining (NHEJ) end capture as the mechanisms underlying correction, the fact that our studies were conducted in neonatal mice, where HDR is permissive and favored as a repair pathway,[39] suggests that the functional repair of hepatocytes is most likely the result of HDR with minimal NHEJ end capture. In aggregate, our results demonstrate that genome editing at the *albumin* start codon has the potential to correct the disease phenotypes with immediacy due to the promoter contained in the AAV donor 5′ homology arm, followed by subsequent durability from integration into *albumin*. Patients with

unpaired Student's t test as mean ± SD. Methylmalonic acid values at 1 month in treated *Mmut*$^{p.G715V/p.G715V}$ mice (690.5 ± 130.9 μM) were comparable with untreated *Mmut*$^{p.G715V/p.G715V}$ (820.3 ± 92.6 μM), but were significantly reduced in treated mice for later time points. *$p < 0.05$, **$p < 0.01$, ***$p < 0.001$, versus the untreated *Mmut*$^{p.G715V/p.G715V}$ group. In (C), weight values are expressed as mean ± SD and analyzed by unpaired Student's t test. In (E), *MMUT* mRNA expression was quantified as percentage of hepatocytes stained positive and expressed as mean ± SEM. At 9 months, edited *Mmut*$^{p.G715V/p.G715V}$ mice exhibited 41.85% ± 4.90% *MMUT*-positive cells in the liver. The treated *Mmut*$^{+/p.G715V}$ control exhibited 9.69% of hepatocytes with positive mRNA staining at this time point.

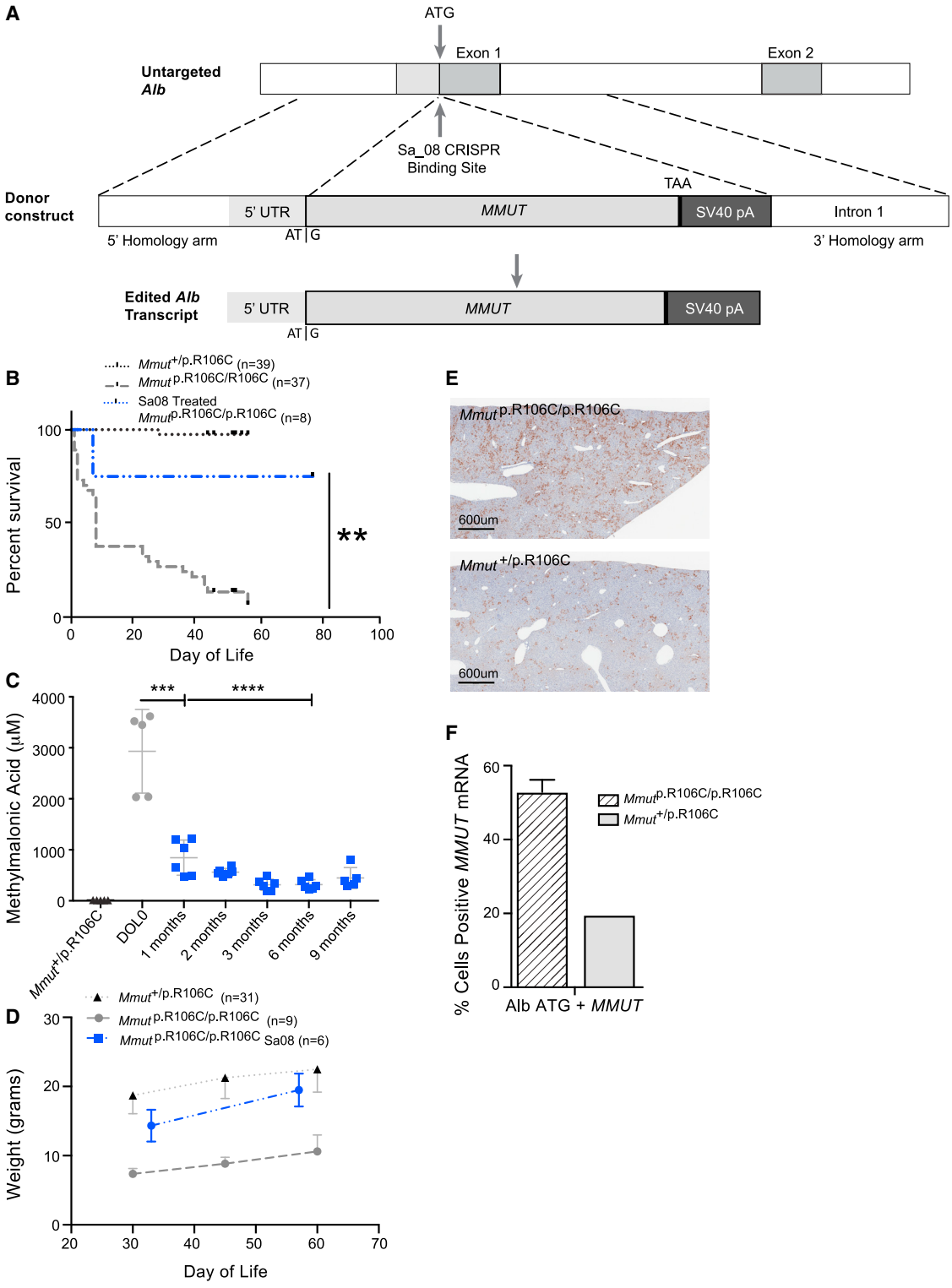

Figure 4. AAV8.MMUT.SV40 targeted to the *Alb* ATG leads to increased *MMUT* mRNA and MMUT protein expression and rescues *Mmut*$^{p.R106C/p.R106C}$ mice from disease lethality

(A) Donor construct corresponding to the gRNA targeting the *Alb* start codon (Sa08). The left homology arm contains the *Alb* 5′ UTR, including part of the *albumin* promoter. (B) Survival of untreated *Mmut*$^{p.R106C/p.R106C}$ and *Mmut*$^{p.R106C/p.R106C}$ administered 5e10 GC/pup AAV8.HLP.SaCas9.Sa08 + 2 × 10^{11} GC/pup AAV8.MMUT.SV40 at birth.

(legend continued on next page)

both severe and intermediate MMUT deficiencies could be treated using an integrating, nuclease-free approach, with a perhaps a preference toward treating more severe mut^0 patients very early in life given the potential for substantial subsequent expansion *in vivo*, which is supported by the striking efficacy in the Mmut R106C mouse model.

Although promising, our studies possess limitations. Off-target and inactivating cleavage by the Cas9 nuclease with any guide targeting *albumin* remains possible. Although the physiological consequences of extreme analbuminemia are well tolerated in some species,[40] even humans,[41] cleavage without recombination of the donor construct could lead to loss of expression of *Alb*, but would require extensive, biallelic inactivation via editing to fully disable a targeted cell's ability to produce albumin. Future studies should aim to improve the design of the donor cassette to restore albumin expression after successful targeting. In addition, alternative means to deliver the Cas9, such as RNA lipid nanoparticles,[42–44] to avoid immune complications and to avoid potential toxicity due to the high doses of AAV required, seems prudent.[16] Nevertheless, our proof-of-concept studies demonstrate that nuclease-enhanced, as well as nuclease-free genome editing at the 5′ end of the *albumin* locus, in multiple positions, including the start codon, are promising treatments for MMA, and might be generally extended to other related metabolic disorders where hepatic correction is needed.

MATERIALS AND METHODS

Generation of MMA mouse models using genome editing

Benchling (http://www.benchling.com) was used to identify protospacer-adjacent motif (PAM) sequences (NGG) from the *Streptococcus pyogenes* (SpyCas9) within ten nucleotides of the desired site for targeted mutagenesis in *Mmut*. gRNAs were synthesized as custom synthetic single-guide RNAs (sgRNAs) (Edit-R predesigned synthetic sgRNA, Horizon Discovery):

Mmut p.R106C (5′-TACTAAAGCCTGCATACTGA -3′)

Mmut p.G715V(5′-TATGAATTTCTGTATGAAGT -3′)

Single-stranded donor oligo sequences containing the desired mutation were co-injected with the Cas9 and sgRNA. For the Mmut p.R106C mutation, a repair template was designed with 80 bp homology arms on either side of the mutation, which was located in the PAM. For the Mmut p.G715V mutation, an asymmetric donor oligo was designed using DeskGen software, with 92 bp left HA and 43 bp right HA. A silent C > A mutation was introduced in the PAM to prevent Cas9 cleavage of the donor construct.

Injected zygotes were cultured at 37°C under 5% CO_2 until blastocyst stage then transferred into the uterus of pseudopregnant females. Murine experiments were approved and performed according to the regulations and standards of the National Human Genome Research Institute (NHGRI) (Bethesda, MD) Animal Care and Use Committee.

Founder genotyping

DNA was extracted from tail clips using the DNeasy Blood & Tissue Kit (QIAGEN) for PCR amplification. ddPCR probes (Bio-Rad) were designed to identify the Mmut p.R106C and Mmut p.G715V mutation sequences. DNA samples from founders were screened by fPCR (for gene knockout) and ddPCR (for HDR of mutation sequences), and crossed with wild-type mice to generate heterozygous carriers of the mutation, which were further bred.

Fluorescent PCR primers

p.R106C_Fwd_fl (5′-TGTAAAACGACGGCCAGTTTCCAGGAGT GAAGCCATTC-3′), p.R106C_Rev_fl (5′- GTGTCTTGCATCCACT TGTTTCACAGC-3′), p.G715V_Fwd_fl (5′- TGTAAAACGACGGC CAGTCAGCTCCACATACAGTGTTCC-3′), and p.G715V_Rev_fl (5′-GTGTCTTTCATCAAGCACTTGGACAGCA-3′).

Identification of SaCas9 guide sequences and *in vitro*/*in vivo* NHEJ testing

To identify sites amenable to genome editing in *Alb,* the first exon and first intron of *Alb* were searched for PAM sequences (NNGRRT) of *S. aureus* Cas9 (SauCas9). The *in vitro* activity of the output 20-nucleotide protospacer guide RNA (gRNA) sequences was measured by transfection of plasmids into mouse carcinoma cell lines. Multiple cell lines, including NIH 3T3 (murine embryonic fibroblastoma), Neuro2A (neuroblastoma), and hepatoma (Hepa1-6) were tested to determine which could provide optimal delivery efficiency by standard transfection and nucleofection methods. Lipofectamine 2000 for standard lipofection was used. For Neuro2A transfections, a ratio of 2:1 (μL of lipofectamine 2000 to μg of DNA) was used, and for

The survival curve depicts the same control cohort of *Mmut*$^{p.R106C/p.R106C}$ and *Mmut*$^{p.R106C/+}$ mice presented in Figure 1E. (C) Plasma methylmalonic acid concentrations for *Mmut*$^{p.R106C/p.R106C}$ treated with 5e10 GC/pup AAV8.HLP.SaCas9.Sa08 + 2×10^{11} GC/pup AAV8.MMUT.SV40 at 1, 2, 3, 6, and 9 months (terminal); concentrations from untreated *Mmut*$^{p.R106C/p.R106C}$ euthanized at birth were used as controls. (D) Weights of untreated *Mmut*$^{p.R106C/p.R106C}$ and untreated *Mmut*$^{+/p.R106C}$ compared with *Mmut*$^{p.R106C/p.R106C}$ treated with the gRNA targeting the *Alb* start codon and donor. Treated *Mmut*$^{p.R106C/p.R106C}$ were significantly larger than untreated *Mmut*$^{p.R106C/p.R106C}$ at both time points, and were not significantly different in size from *Mmut*$^{+/p.R106C}$ by age 1 month. (E) Liver sections from treated *Mmut*$^{p.R106C/p.R106C}$ mice euthanized at 9 months post-treatment were stained for *MMUT* mRNA. (F) Expression of the *MMUT* mRNA at 9 months in treated *Mmut*$^{p.R106C/p.R106C}$ mice was evenly distributed throughout the liver. The treated *Mmut*$^{+/p.R106C}$ control exhibited fewer cells with positive *MMUT* mRNA staining at the same time point. In (B), data were analyzed by log rank Mantel-Cox and Gehan-Breslow-Wilcoxon test. **$p < 0.01$, versus the untreated *Mmut*$^{p.R106C/p.R106C}$ group. In (C), plasma methylmalonic acid concentrations were analyzed by unpaired Student's t test as mean ± SD. Methylmalonic acid values were significantly reduced at 1 month in treated *Mmut*$^{p.R106C/p.R106C}$ mice compared with untreated neonatal *Mmut*$^{p.R106C/p.R106C}$ controls, and were further reduced for all later time points. ***$p < 0.001$, ****$p < 0.0001$, versus the untreated *Mmut*$^{p.R106C/p.R106C}$ group. In (D), weight values are expressed as mean ± SD. In (F), *MMUT* mRNA expression was quantified as percentage of hepatocytes stained positive and expressed as mean ± SEM. At 9 months edited *Mmut*$^{p.R106C/p.R106C}$ mice exhibited 52.89% ± 1.46% *MMUT*-positive cells in the liver. The treated *Mmut*$^{+/p.R106C}$ control exhibited 19.57% of hepatocytes with positive mRNA staining at this time point.

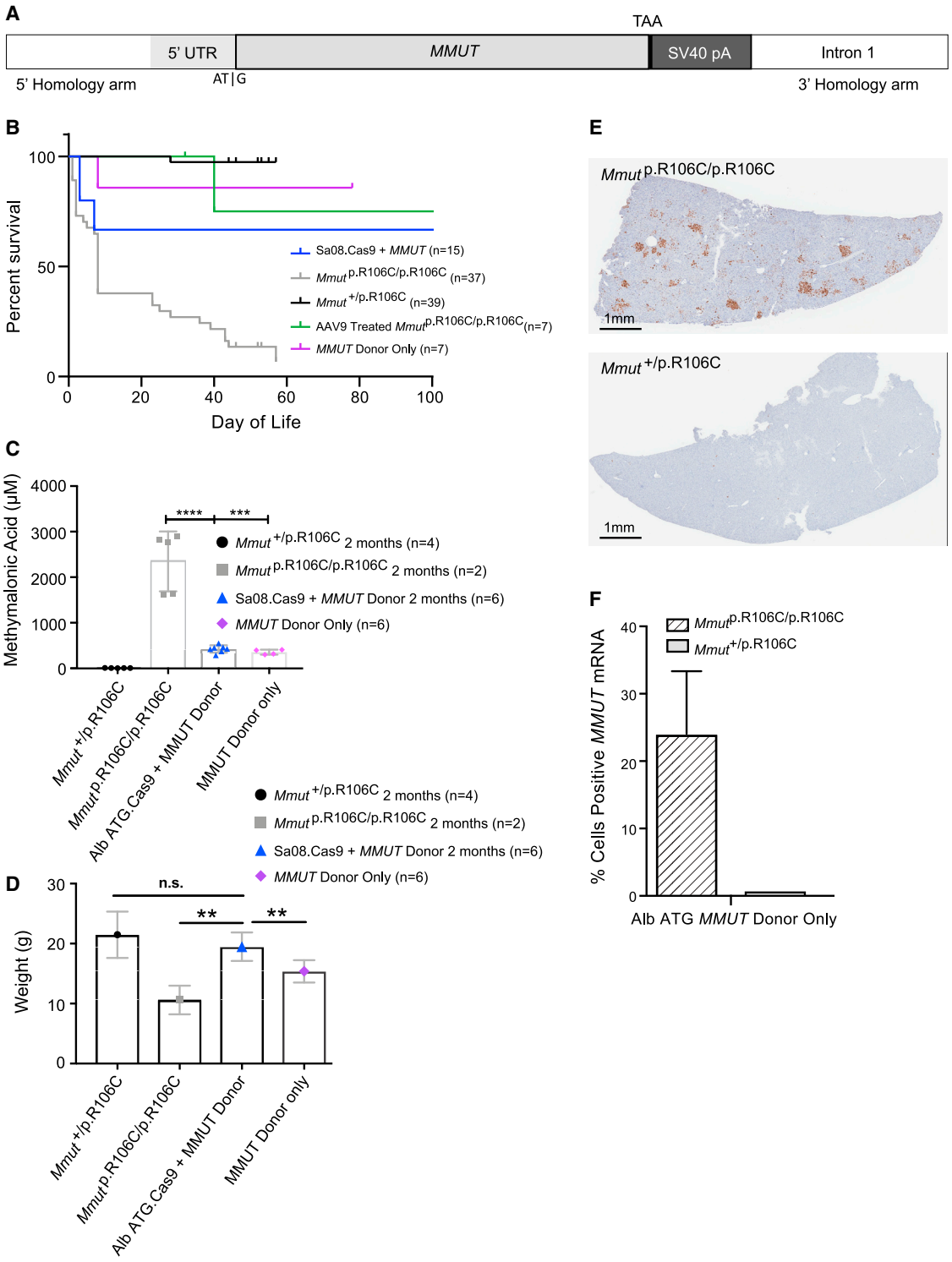

Figure 5. Nuclease-free editing with AAV8.MMUT.SV40 results in *MMUT* mRNA expression and improves survival, growth, and methylmalonic acid concentrations in *Mmut*$^{p.R106C/p.R106C}$ mice

(A) Donor construct corresponding to the gRNA targeting the *Alb* start codon (Sa08). (B) Survival of *Mmut*$^{p.R106C/p.R106C}$ mice treated at birth with either the dual 5e10 GC/pup AAV8.HLP.SaCas9.Sa08 + 2 × 10^{11} GC/pup AAV8.MMUT.SV40 (blue), with 2 × 10^{11} GC/pup of the AAV8.MMUT.SV40 donor vector only (purple), or with 1e11 GC/pup

(legend continued on next page)

Hepa1-6 transfections, a ratio of 3:1 was used. Cells were seeded in 24-well plates 24 h prior to transfection; 1 μg of plasmid DNA was transfected per well.

For the T7E1 assay, primers were designed to amplify a 500- to 800-bp region centered on the gRNA target. High-fidelity Accuprime Taq from Life Technologies was used for all PCR experiments. PCR was run for 40 cycles to ensure sufficient product. The PCR reaction was purified and normalized to 12 ng/μL; 16.2 μL (~200 ng) of the 12 ng/μL PCR product was mixed with 1.8 μL of 10X NEB buffer 2 for a final volume of 18 μL. DNA was melted and re-annealed by placing in a thermocycler for 10 min at 95°C, then decreasing at 0.1°C/s down to 25°C. Two microliters of an enzyme master mix (0.5 μL T7EI, 0.2 μL NEB buffer 2, and 1.3 μL water) was added to each reaction and immediately placed in a thermocycler at 37°C for 60 min. After 60 min, the reactions were immediately removed from the thermocycler and quenched by adding EDTA to a final concentration of 45 mM. A quenching loading dye composed of 0.5 M EDTA and 6X DNA loading dye at a ratio of 1:2 EDTA:dye was used. The full content of the samples was immediately loaded into a 2% agarose gel and run until the bands were well separated.

Off-target analysis and deep sequencing

The bioinformatic tool CRISPR off-target sites with mismatches, insertions, and/or deletions (COSMID)[45] was used to search the *Mus musculus* (Mm10 build) genome for chromosomal locations similar to the guide RNA with a maximum of three mismatches and an NNGRRT PAM. Mouse liver genomic DNA was extracted using the QIAGEN Blood & Tissue Kit, and target sequences were amplified using site-specific primers containing common adaptor sequences. A second round of PCR was used to add custom Illumina sample indexes. Both rounds of PCR were performed using five touchdown cycles with the annealing temperatures decreasing each round by 1°C from 65°C to 60°C. Target amplicons were purified using magnetic beads, pooled in equimolar amounts, and sequenced using the Illumina MiSeq platform. Alignment of sequence reads to reference sequences was performed as described previously,[46] and indels overlapping a ±2-base pair window around the cut site were quantified.

SaCas9 expression cassettes

The AAV.HLP.SauCas9.U6.gRNA construct used for *in vivo* experiments was described previously.[23] Oligos containing the gRNA sequence and restriction enzyme overhangs were resuspended in distilled water to a concentration of 10 μM. Oligos (0.8 μL) were phosphorylated in a 25-μL reaction, then mixed before annealing for 1 h (50 μL). One microliter of annealed oligos plus 12.5 ng of vector were ligated in a 10-μL ligation reaction (25 μL *E. coli*, 175 μL SOC, and all 200 μL were plated). The gRNA oligo sequences for sites targeting intron 1 of *albumin* (Sa37) and the ATG of *albumin* (Sa08) are as follows (the 5′ base was replaced by a "g" for U6 promoter expression):

Sa_08_T:CACCgCTAGCCTCTGGCAAAATGAA

Sa_08_B:AAACTTCATTTTGCCAGAGGCTAGc

Sa_37_T:CACCgTGCACAGATATAAACACTTA

Sa_37_B:AAACTAAGTGTTTATATCTGTGCAc

Donor construct design

Donor constructs were designed for Sa37 and Sa08 gRNA targets. A full-length, human codon-optimized methylmalonyl-CoA mutase cDNA (*MMUT*) was preceded by a 2A peptide or an IRES sequence. The 2A peptide sequence was preceded by the two nucleotides coding for histidine, the 27th amino acid in *Alb*, to maintain the reading frame. A polypyrimidine tract and splice acceptor were additionally added to the 5′ end of the insert. A synthetic SV40 poly(A) tail was

AAV9.EF1a.PI.MMUT.RBG (green) compared with untreated $Mmut^{+/p.R106C}$ and $Mmut^{p.R106C/p.R106C}$ mice. $Mmut^{p.R106C/p.R106C}$ mice treated with only the AAV8.MMUT.SV40 donor survived to DOL78 and did not show significantly different survival from healthy $Mmut^{+/p.R106C}$ controls. To compare treated $Mmut^{p.R106C/p.R106C}$ mice to untreated controls, which do not survive beyond DOL60, only time points for survival and weights were included for which control data were available. The survival curve depicts the same control cohort of $Mmut^{p.R106C/p.R106C}$ and $Mmut^{p.R106C/+}$ mice presented in Figure 1E. (C) Plasma methylmalonic acid concentrations for $Mmut^{p.R106C/p.R106C}$ (n = 4) treated with AAV8.MMUT.SV40 donor-only (purple) at 2 months post-treatment, compared with $Mmut^{p.R106C/p.R106C}$ treated with Cas9 + donor at the same time point (n = 7). Untreated $Mmut^{p.R106C/p.R106C}$ euthanized at birth (n = 5) and untreated $Mmut^{+/p.R106C}$ (n = 5) were used as controls. Methylmalonic acid values in donor-only-treated mice were significantly reduced compared with untreated $Mmut^{p.R106C/p.R106C}$, and were not significantly different from $Mmut^{p.R106C/p.R106C}$ treated with Cas9 + donor. (D) Weights of $Mmut^{p.R106C/p.R106C}$ treated with Cas9 + donor vectors (blue), or AAV8.MMUT.SV40 donor-only (purple) at age 2 months, compared with untreated $Mmut^{+/p.R106C}$ and surviving untreated $Mmut^{p.R106C/p.R106C}$. Donor-only-treated $Mmut^{p.R106C/p.R106C}$ were significantly larger than untreated $Mmut^{p.R106C/p.R106C}$ at 2 months, but were smaller in size than $Mmut^{p.R106C/p.R106C}$ treated with Cas9 + donor. (E) To assess genome editing following treatment with the donor-only vector, liver sections from treated $Mmut^{p.R106C/p.R106C}$ mice euthanized at 5 months post-treatment were stained for *MMUT* mRNA. (F) Expression of the *MMUT* transgene at 5 months in $Mmut^{p.R106C/p.R106C}$ (n = 4), with discreet clusters of positively stained cells dispersed throughout the liver. One treated $Mmut^{+/p.R106C}$ control exhibited almost no cells positive for mRNA staining at 5 months. In (B), 85.71% (n = 7) $Mmut^{p.R106C/p.R106C}$ mice treated with only the AAV8.MMUT.SV40 donor survived to DOL78 and did not show significantly different survival from healthy $Mmut^{+/p.R106C}$ controls (log rank [Mantel-Cox] and Gehan-Breslow-Wilcoxon tests). In (C), plasma methylmalonic acid concentrations were analyzed by unpaired Student's t test as mean ± SD. Methylmalonic acid values in donor-only-treated mice were significantly reduced compared with untreated $Mmut^{p.R106C/p.R106C}$ ($p = 0.0006$, unpaired t test), and were not significantly different from $Mmut^{p.R106C/p.R106C}$ treated with Cas9 + donor (unpaired t test). ***$p < 0.001$, ****$p < 0.0001$. In (D), weight values are expressed as mean ± SD. Donor-only-treated $Mmut^{p.R106C/p.R106C}$ were significantly larger than untreated $Mmut^{p.R106C/p.R106C}$ at 2 months ($p < 0.05$), but were smaller in size than $Mmut^{p.R106C/p.R106C}$ treated with Cas9 + donor ($p < 0.01$). **$p < 0.01$, n.s., not significant. In (F), *MMUT* mRNA expression was quantified as percentage of hepatocytes stained positive and expressed as mean ± SEM. Expression of the *MMUT* transgene at 5 months in $Mmut^{p.R106C/p.R106C}$ (n = 4) averaged 24.05% ± 4.65%, with rosettes of positively stained cells throughout the liver. One treated $Mmut^{+/p.R106C}$ control exhibited almost no cells positive for mRNA staining at 5 months (0.81%).

added to the 3′ end of *MMUT*. Homology arms were designed to be at least 400 bp when possible; the *albumin* intron 1 target (Sa37) 3′ homology arm was truncated due to a complex repeat region in the mouse genome in intron 2 of *Alb*. For the donor construct corresponding to the gRNA that targets the *Alb* transcriptional start site (Sa08), the *MMUT* cDNA was full-length except for the first two nucleotides (the AT of the ATG of *Alb*), which were contained in the 5′ homology arm containing the *Alb* 5′ UTR. The final cassettes were sequenced using NGS to validate before use.

Recombinant AAV vector production

A dual-vector system was adopted to deliver genome-editing components using AAV serotype 8 vectors. One vector (AAV8.HLP.SauCas9) co-expressed the SauCas9 gene from a human liver-specific promoter and the sgRNA scaffold sequence expressed from the U6 promoter; the second vector (AAV8.donor) contained a human codon-optimized MMUT cDNA. Pups were injected on DOL0 or DOL1 with a ratio of 1:4 of the AAV8.HLP.SauCas9 (5e10 GC/g) to the AAV8.donor (2e11 GC/g). AAV8 vectors were produced using standard methods at either Baylor College of Medicine (Dr. William Lagor's lab) or by the Vector Core at University of Massachusetts Medical School (Dr. Guangping Gao's lab).

Another set of AAV vectors, AAV8.EF1a.PI.MMUT.RBG or AAV9.EF1a.PI.MMUT.RBG were prepared by University of Pennsylvania's Vector Core as described previously.[11,13]

Methylmalonic acid measurement

Plasma was isolated from blood collected by orbital bleeding. Samples were stored at −80°C until analysis by gas chromatography-mass spectrometry to measure methylmalonic acid concentration, as described previously.[47]

Animal studies

Animal work was performed in accordance with the guidelines for animal care at NIH. Both mouse models were on a mixed C57BL/6 × 129SV/Ev × FvBN genetic background. Experimental groups contained equal numbers of both genders. Treated mice received AAV via intrahepatic injection on day 0 or day 1. Mice were bled via retro-orbital sinus plexus sampling using a sterile glass capillary tube and weighed monthly.

Western blot analysis

Samples were prepared and run according to standard protocols. The following antibodies were used for the detection of MMUT (Abcam, ab134956), β-actin (Abcam, ab8227) in conjunction with the following secondary antibodies (LI-COR, 925-32211) and (LI-COR, 926-68072).

Hepatic *MMUT* RNA *in situ* hybridization

RNAscope probes were designed against the human codon-optimized *MMUT* RNA by ACDBio using their proprietary technology and do not cross-react with other transcripts in the murine transcriptome, including *Mmut*. Livers were fixed in 4% PFA and processed into paraffin blocks. Five-micron sections were cut and stained with the RNAScope 2.5 HD Assay-Brown (ACDBio 322300) following the manufacturer's instructions. Slide images were captured using the Zeiss AxioScan Z1 slide scanner and analyzed using Image-Pro premier 3D version 9.3 by Media Cybernetics.

Vector genome quantitation

Genomic DNA from liver samples was extracted using DNeasy Blood & Tissue Kit (QIAGEN; 69506) following the manufacturer's procedures. ddPCR was performed according to the manufacturer's recommendations for the Bio-Rad QX200 AutoDG ddPCR system using 10 or 20 ng of DNA as input and the following probes: Bio-Rad ddPCR CNV assay *Gapdh* (cat no. 10042961, dMumCNS300520369) and *MMUT* (cat no. 10042958 dCNS513322846).

Albumin integration assay

Genomic DNA from liver samples was extracted using DNeasy Blood & Tissue Kit (QIAGEN; 69504) following the manufacturer's procedures. A PCR product representing the genomic integration between the *Alb* locus and 5′ end of the *MMUT* donor construct indicated on-target integration. gDNA (200 ng) from various mouse liver samples was used as template for the DNA integration assay.

Statistical analyses

Prism 8 by GraphPad was used to analyze all data. Results are expressed as mean ± SD/SEM. Values of $p < 0.05$ were considered statistically significant. Where animal injections were unsuccessful, as determined by vector genome copies in liver, data were excluded. Depending on the experimental design, an unpaired t test, or log rank (Mantel-Cox) test was used as indicated in the legends to the figures. The statistical analysis performed for each dataset is indicated in the figure legends. For all figures, *$p < 0.05$, **$p < 0.01$, ***$p < 0.001$, ****$p < 0.0001$, except where different symbols were used.

SUPPLEMENTAL INFORMATION

Supplemental information can be found online at https://doi.org/10.1016/j.omtm.2021.11.004.

ACKNOWLEDGMENTS

The expert assistance from Darwin Romero with animal husbandry and care, and other members of the NHGRI laboratory and animal support program, was critical to this work. R.J.C., L.E.V., and C.P.V. were supported by the Intramural Research Program of the NHGRI through 1ZIAHG200318-16. J.L.S. and S.M. were supported, in part, by the Angels for MMA Research Fund, the Cure for Clark Fund, and the Organic Acidemia Association Research Fund. W.R.L. and A.E.H. were supported by the following grants from NIH: HL132840, U42OD026645, and UG3HL151545. G.B. was supported in part by NIH grants UG3HL151545 and R01HL152314.

AUTHOR CONTRIBUTIONS

Conceptualization, J.L.S. and C.P.V.; methodology, T.J.C., J.L.S., A.E.H., W.R.L., C.M.L., and C.P.V.; software, T.J.C. and A.L.; validation, A.E.H., W.R.L., C.M.L., and L.E.V.; formal analysis, J.L.S.,

C.M.L., and A.L.; investigation, J.L.S., C.M.L., A.L., S.M., and L.E.V.; resources, A.E.H., W.R.L., A.L., and C.P.V.; writing – original draft, J.L.S. and C.P.V.; writing – review & editing, A.E.H., W.R.L., C.M.L., A.L., T.J.C., L.E.V., S.M., R.J.C., and C.P.V.; visualization, J.L.S. and C.M.L.; supervision, G.B., W.R.L., and C.P.V.; project administration, J.L.S., C.M.L., W.R.L., and C.P.V.; funding acquisition, W.R.L., G.B., and C.P.V.

DECLARATION OF INTERESTS

The authors declare no competing interests.

REFERENCES

1. Manoli, I., Sloan, J.L., and Venditti, C.P. (2005). Isolated methylmalonic acidemia. In GeneReviews((R)), M.P. Adam, H.H. Ardinger, R.A. Pagon, S.E. Wallace, L.J.H. Bean, and K. Stephens, et al., eds. (Seattle: University of Washington), pp. 1993–2021.
2. Kolker, S., Cazorla, A.G., Valayannopoulos, V., Lund, A.M., Burlina, A.B., Sykut-Cegielska, J., Wijburg, F.A., Teles, E.L., Zeman, J., Dionisi-Vici, C., et al. (2015). Erratum to: the phenotypic spectrum of organic aciduria and urea cycle disorders. Part 1: the initial presentation. J. Inherit. Metab. Dis. *38*, 1155–1156. https://doi.org/10.1007/s10545-015-9867-z.
3. Manoli, I., Myles, J.G., Sloan, J.L., Shchelochkov, O.A., and Venditti, C.P. (2016). A critical reappraisal of dietary practices in methylmalonic acidemia raises concerns about the safety of medical foods. Part 1: isolated methylmalonic acidemias. Genet. Med. *18*, 386–395. https://doi.org/10.1038/gim.2015.102.
4. Fraser, J.L., and Venditti, C.P. (2016). Methylmalonic and propionic acidemias: clinical management update. Curr. Opin. Pediatr. *28*, 682–693. https://doi.org/10.1097/MOP.0000000000000422.
5. Niemi, A.K., Kim, I.K., Krueger, C.E., Cowan, T.M., Baugh, N., Farrell, R., Bonham, C.A., Concepcion, W., Esquivel, C.O., and Enns, G.M. (2015). Treatment of methylmalonic acidemia by liver or combined liver-kidney transplantation. J. Pediatr. *166*, 1455–1461 e51. https://doi.org/10.1016/j.jpeds.2015.01.051.
6. Sloan, J.L., Manoli, I., and Venditti, C.P. (2015). Liver or combined liver-kidney transplantation for patients with isolated methylmalonic acidemia: who and when? J. Pediatr. *166*, 1346–1350. https://doi.org/10.1016/j.jpeds.2015.03.026.
7. van 't Hoff, W.G., Dixon, M., Taylor, J., Mistry, P., Rolles, K., Rees, L., and Leonard, J.V. (1998). Combined liver-kidney transplantation in methylmalonic acidemia. J. Pediatr. *132*, 1043–1044. https://doi.org/10.1016/s0022-3476(98)70407-x.
8. Chu, T.H., Chien, Y.H., Lin, H.Y., Liao, H.C., Ho, H.J., Lai, C.J., Chiang, C.C., Lin, N.C., Yang, C.F., Hwu, W.L., et al. (2019). Methylmalonic acidemia/propionic acidemia—the biochemical presentation and comparing the outcome between liver transplantation versus non-liver transplantation groups. Orphanet J. Rare Dis. *14*, 73. https://doi.org/10.1186/s13023-019-1045-1.
9. Saudubray, J.M., Touati, G., Delonlay, P., Jouvet, P., Schlenzig, J., Narcy, C., Laurent, J., Rabier, D., Kamoun, P., Jan, D., and Revillon, Y. (1999). Liver transplantation in propionic acidaemia. Eur. J. Pediatr. *158* (*Suppl. 2*), S65–S69. https://doi.org/10.1007/pl00014325.
10. Schneller, J.L., Lee, C.M., Bao, G., and Venditti, C.P. (2017). Genome editing for inborn errors of metabolism: advancing towards the clinic. BMC Med. *15*, 43. https://doi.org/10.1186/s12916-017-0798-4.
11. Carrillo-Carrasco, N., Chandler, R.J., Chandrasekaran, S., and Venditti, C.P. (2010). Liver-directed recombinant adeno-associated viral gene delivery rescues a lethal mouse model of methylmalonic acidemia and provides long-term phenotypic correction. Hum. Gene Ther. *21*, 1147–1154. https://doi.org/10.1089/hum.2010.008.
12. Chandler, R.J., and Venditti, C.P. (2012). Pre-clinical efficacy and dosing of an AAV8 vector expressing human methylmalonyl-CoA mutase in a murine model of methylmalonic acidemia (MMA). Mol. Genet. Metab. *107*, 617–619. https://doi.org/10.1016/j.ymgme.2012.09.019.
13. Senac, J.S., Chandler, R.J., Sysol, J.R., Li, L., and Venditti, C.P. (2012). Gene therapy in a murine model of methylmalonic acidemia using rAAV9-mediated gene delivery. Gene Ther. *19*, 385–391. https://doi.org/10.1038/gt.2011.108.
14. An, D., Schneller, J.L., Frassetto, A., Liang, S., Zhu, X., Park, J.S., Theisen, M., Hong, S.J., Zhou, J., Rajendran, R., et al. (2018). Systemic messenger RNA therapy as a treatment for methylmalonic acidemia. Cell Rep. *24*, 2520. https://doi.org/10.1016/j.celrep.2018.08.049.
15. Chandler, R.J., LaFave, M.C., Varshney, G.K., Trivedi, N.S., Carrillo-Carrasco, N., Senac, J.S., Wu, W., Hoffmann, V., Elkahloun, A.G., Burgess, S.M., and Venditti, C.P. (2015). Vector design influences hepatic genotoxicity after adeno-associated virus gene therapy. J. Clin. Invest. *125*, 870–880. https://doi.org/10.1172/JCI79213.
16. Li, A., Tanner, M.R., Lee, C.M., Hurley, A.E., De Giorgi, M., Jarrett, K.E., Davis, T.H., Doerfler, A.M., Bao, G., Beeton, C., and Lagor, W.R. (2020). AAV-CRISPR gene editing is negated by pre-existing immunity to Cas9. Mol. Ther. *28*, 1432–1441. https://doi.org/10.1016/j.ymthe.2020.04.017.
17. Worgan, L.C., Niles, K., Tirone, J.C., Hofmann, A., Verner, A., Sammak, A., Kucic, T., Lepage, P., and Rosenblatt, D.S. (2006). Spectrum of mutations in mut methylmalonic acidemia and identification of a common Hispanic mutation and haplotype. Hum. Mutat. *27*, 31–43. https://doi.org/10.1002/humu.20258.
18. An, D., Frassetto, A., Jacquinet, E., Eybye, M., Milano, J., DeAntonis, C., Nguyen, V., Laureano, R., Milton, J., Sabnis, S., et al. (2019). Long-term efficacy and safety of mRNA therapy in two murine models of methylmalonic acidemia. EBioMedicine *45*, 519–528. https://doi.org/10.1016/j.ebiom.2019.07.003.
19. Chandler, R.J., Sloan, J., Fu, H., Tsai, M., Stabler, S., Allen, R., Kaestner, K.H., Kazazian, H.H., and Venditti, C.P. (2007). Metabolic phenotype of methylmalonic acidemia in mice and humans: the role of skeletal muscle. BMC Med. Genet. *8*, 64. https://doi.org/10.1186/1471-2350-8-64.
20. Chandler, R.J., and Venditti, C.P. (2010). Long-term rescue of a lethal murine model of methylmalonic acidemia using adeno-associated viral gene therapy. Mol. Ther. *18*, 11–16. https://doi.org/10.1038/mt.2009.247.
21. Manoli, I., Sysol, J.R., Epping, M.W., Li, L., Wang, C., Sloan, J.L., Pass, A., Gagne, J., Ktena, Y.P., Li, L., et al. (2018). FGF21 underlies a hormetic response to metabolic stress in methylmalonic acidemia. JCI Insight *3*. https://doi.org/10.1172/jci.insight.124351.
22. Sharma, R., Anguela, X.M., Doyon, Y., Wechsler, T., DeKelver, R.C., Sproul, S., Paschon, D.E., Miller, J.C., Davidson, R.J., Shivak, D., et al. (2015). In vivo genome editing of the albumin locus as a platform for protein replacement therapy. Blood *126*, 1777–1784. https://doi.org/10.1182/blood-2014-12-615492.
23. Jarrett, K.E., Lee, C., De Giorgi, M., Hurley, A., Gillard, B.K., Doerfler, A.M., Li, A., Pownall, H.J., Bao, G., and Lagor, W.R. (2018). Somatic editing of Ldlr with adeno-associated viral-CRISPR is an efficient tool for atherosclerosis research. Arterioscler Thromb. Vasc. Biol. *38*, 1997–2006. https://doi.org/10.1161/ATVBAHA.118.311221.
24. Chandler, R.J., Venturoni, L.E., Liao, J., Hubbard, B.T., Schneller, J.L., Hoffmann, V., Gordo, S., Zang, S., Ko, C.W., Chau, N., et al. (2020). Promoterless, nuclease-free genome editing confers a growth advantage for corrected hepatocytes in mice with methylmalonic acidemia. Hepatology. https://doi.org/10.1002/hep.31570.
25. Peters, H., Nefedov, M., Sarsero, J., Pitt, J., Fowler, K.J., Gazeas, S., Kahler, S.G., and Ioannou, P.A. (2003). A knock-out mouse model for methylmalonic aciduria resulting in neonatal lethality. J. Biol. Chem. *278*, 52909–52913. https://doi.org/10.1074/jbc.M310533200.
26. Chandler, R.J., Zerfas, P.M., Shanske, S., Sloan, J., Hoffmann, V., DiMauro, S., and Venditti, C.P. (2009). Mitochondrial dysfunction in mut methylmalonic acidemia. FASEB J. *23*, 1252–1261. https://doi.org/10.1096/fj.08-121848.
27. Peters, H.L., Pitt, J.J., Wood, L.R., Hamilton, N.J., Sarsero, J.P., and Buck, N.E. (2012). Mouse models for methylmalonic aciduria. PLoS One *7*, e40609. https://doi.org/10.1371/journal.pone.0040609.
28. Buck, N.E., Dashnow, H., Pitt, J.J., Wood, L.R., and Peters, H.L. (2012). Development of transgenic mice containing an introduced stop codon on the human methylmalonyl-CoA mutase locus. PLoS One *7*, e44974. https://doi.org/10.1371/journal.pone.0044974.
29. Forny, P., Schumann, A., Mustedanagic, M., Mathis, D., Wulf, M.A., Nagele, N., Langhans, C.D., Zhakupova, A., Heeren, J., Scheja, L., et al. (2016). Novel mouse models of methylmalonic aciduria recapitulate phenotypic traits with a genetic dosage effect. J. Biol. Chem. *291*, 20563–20573. https://doi.org/10.1074/jbc.M116.747717.

30. Manoli, I., Sysol, J.R., Li, L., Houillier, P., Garone, C., Wang, C., Zerfas, P.M., Cusmano-Ozog, K., Young, S., Trivedi, N.S., et al. (2013). Targeting proximal tubule mitochondrial dysfunction attenuates the renal disease of methylmalonic acidemia. Proc. Natl. Acad. Sci. U S A *110*, 13552–13557. https://doi.org/10.1073/pnas.1302764110.

31. Laoharawee, K., DeKelver, R.C., Podetz-Pedersen, K.M., Rohde, M., Sproul, S., Nguyen, H.O., Nguyen, T., St Martin, S.J., Ou, L., Tom, S., et al. (2018). Dose-dependent prevention of metabolic and neurologic disease in murine MPS II by ZFN-mediated in vivo genome editing. Mol. Ther. *26*, 1127–1136. https://doi.org/10.1016/j.ymthe.2018.03.002.

32. Ou, L., Przybilla, M.J., Ahlat, O., Kim, S., Overn, P., Jarnes, J., O'Sullivan, M.G., and Whitley, C.B. (2020). A highly efficacious PS gene editing system corrects metabolic and neurological complications of mucopolysaccharidosis type I. Mol. Ther. *28*, 1442–1454. https://doi.org/10.1016/j.ymthe.2020.03.018.

33. Barzel, A., Paulk, N.K., Shi, Y., Huang, Y., Chu, K., Zhang, F., Valdmanis, P.N., Spector, L.P., Porteus, M.H., Gaensler, K.M., and Kay, M.A. (2015). Promoterless gene targeting without nucleases ameliorates haemophilia B in mice. Nature *517*, 360–364. https://doi.org/10.1038/nature13864.

34. De Caneva, A., Porro, F., Bortolussi, G., Sola, R., Lisjak, M., Barzel, A., Giacca, M., Kay, M.A., Vlahovicek, K., Zentilin, L., and Muro, A.F. (2019). Coupling AAV-mediated promoterless gene targeting to SaCas9 nuclease to efficiently correct liver metabolic diseases. JCI Insight *5*. https://doi.org/10.1172/jci.insight.128863.

35. Porro, F., Bortolussi, G., Barzel, A., De Caneva, A., Iaconcig, A., Vodret, S., Zentilin, L., Kay, M.A., and Muro, A.F. (2017). Promoterless gene targeting without nucleases rescues lethality of a Crigler-Najjar syndrome mouse model. EMBO Mol. Med. *9*, 1346–1355. https://doi.org/10.15252/emmm.201707601.

36. Lisowski, L., Dane, A.P., Chu, K., Zhang, Y., Cunningham, S.C., Wilson, E.M., Nygaard, S., Grompe, M., Alexander, I.E., and Kay, M.A. (2014). Selection and evaluation of clinically relevant AAV variants in a xenograft liver model. Nature *506*, 382–386. https://doi.org/10.1038/nature12875.

37. Nygaard, S., Barzel, A., Haft, A., Major, A., Finegold, M., Kay, M.A., and Grompe, M. (2016). A universal system to select gene-modified hepatocytes in vivo. Sci. Transl. Med. *8*, 342–379. https://doi.org/10.1126/scitranslmed.aad8166.

38. Borel, F., Tang, Q., Gernoux, G., Greer, C., Wang, Z., Barzel, A., Kay, M.A., Shultz, L.D., Greiner, D.L., Flotte, T.R., et al. (2017). Survival advantage of both human hepatocyte xenografts and genome-edited hepatocytes for treatment of alpha-1 antitrypsin deficiency. Mol. Ther. *25*, 2477–2489. https://doi.org/10.1016/j.ymthe.2017.09.020.

39. Yang, Y., Wang, L., Bell, P., McMenamin, D., He, Z., White, J., Yu, H., Xu, C., Morizono, H., Musunuru, K., et al. (2016). A dual AAV system enables the Cas9-mediated correction of a metabolic liver disease in newborn mice. Nat. Biotechnol. *34*, 334–338. https://doi.org/10.1038/nbt.3469.

40. Roopenian, D.C., Low, B.E., Christianson, G.J., Proetzel, G., Sproule, T.J., and Wiles, M.V. (2015). Albumin-deficient mouse models for studying metabolism of human albumin and pharmacokinetics of albumin-based drugs. MAbs *7*, 344–351. https://doi.org/10.1080/19420862.2015.1008345.

41. Minchiotti, L., Caridi, G., Campagnoli, M., Lugani, F., Galliano, M., and Kragh-Hansen, U. (2019). Diagnosis, phenotype, and molecular genetics of congenital analbuminemia. Front Genet. *10*, 336. https://doi.org/10.3389/fgene.2019.00336.

42. Wang, M., Zuris, J.A., Meng, F., Rees, H., Sun, S., Deng, P., Han, Y., Gao, X., Pouli, D., Wu, Q., et al. (2016). Efficient delivery of genome-editing proteins using bioreducible lipid nanoparticles. Proc. Natl. Acad. Sci. U S A *113*, 2868–2873. https://doi.org/10.1073/pnas.1520244113.

43. Miller, J.B., Zhang, S., Kos, P., Xiong, H., Zhou, K., Perelman, S.S., Zhu, H., and Siegwart, D.J. (2017). Non-viral CRISPR/Cas gene editing in vitro and in vivo enabled by synthetic nanoparticle Co-delivery of Cas9 mRNA and sgRNA. Angew. Chem. Int. Ed. Engl. *56*, 1059–1063. https://doi.org/10.1002/anie.201610209.

44. Yin, H., Song, C.Q., Dorkin, J.R., Zhu, L.J., Li, Y., Wu, Q., Park, A., Yang, J., Suresh, S., Bizhanova, A., et al. (2016). Therapeutic genome editing by combined viral and non-viral delivery of CRISPR system components in vivo. Nat. Biotechnol. *34*, 328–333. https://doi.org/10.1038/nbt.3471.

45. Cradick, T.J., Qiu, P., Lee, C.M., Fine, E.J., and Bao, G. (2014). COSMID: a web-based tool for identifying and validating CRISPR/Cas off-target sites. Mol. Ther. Nucleic Acids. https://doi.org/10.1038/mtna.2014.64.

46. Lin, Y., Cradick, T.J., Brown, M.T., Deshmukh, H., Ranjan, P., Sarode, N., Wile, B.M., Vertino, P.M., Stewart, F.J., and Bao, G. (2014). CRISPR/Cas9 systems have off-target activity with insertions or deletions between target DNA and guide RNA sequences. Nucleic Acids Res. *42*, 7473–7485. https://doi.org/10.1093/nar/gku402.

47. Marcell, P.D., Stabler, S.P., Podell, E.R., and Allen, R.H. (1985). Quantitation of methylmalonic acid and other dicarboxylic acids in normal serum and urine using capillary gas chromatography-mass spectrometry. Anal Biochem. *150*, 58–66. https://doi.org/10.1016/0003-2697(85)90440-3.